Int. J. Sci. R. Tech., 2026 3(8)
A Multidisciplinary peer-reviewed Journal
www.ijsrtjournal.com [ISSN: 2394-7063]

Original Article

Design, Synthesis, Characterization And In Vitro Antileishmanial Evaluation Of 2,4,6-Substituted Pyrimidine Derivatives Conjugated With Imidazole Moieties

Dipraj Kochak*, Archana Tiwari, Shikha Nagle, Dishant Gupta

Swami Vivekanand college of Pharmacy, Indore

ABSTRACT

The present study describes the design, synthesis, preliminary characterization, and *in vitro* antileishmanial evaluation of a focused series of imidazole-conjugated 2,4,6-substituted pyrimidine derivatives designated UG-1 to UG-10. The compounds were designed through scaffold hybridization involving a substituted imidazole moiety, a *para*-phenylene linker, and a 2-aminopyrimidine core bearing electronically diverse aryl substituents. The synthetic route comprised three sequential stages: nucleophilic aromatic substitution of 2-substituted imidazoles with 4-fluorobenzaldehyde in dry *N,N*-dimethylformamide using potassium carbonate and hexadecyltrimethylammonium bromide; Claisen–Schmidt condensation of the resulting aldehyde intermediates with substituted acetophenones; and cyclocondensation of the chalcone intermediates with guanidine hydrochloride in ethanolic sodium hydroxide. The target derivatives were obtained in yields ranging from 55% to 85%. Thin-layer chromatography produced Rf values between 0.130 and 0.80, indicating differences in chromatographic behaviour across the compound series. FT-IR analysis provided functional-group-level evidence for the presence of amino, aromatic, imine, cyano, nitro, methoxy, and chloro functionalities in the relevant derivatives. Biological evaluation identified UG-9, an ethyl-imidazole derivative containing a 3-chlorophenyl substituent, as the most promising compound in the supplied dataset. UG-9 exhibited IC_{50} values of 11.2 µM against *Leishmania* promastigotes and 8.6 µM against intracellular amastigotes. Cytotoxicity evaluation against RAW 264.7 macrophages produced a CC_{50} value of 126.4 µM, corresponding to an intracellular amastigote-based selectivity index of 14.7. These findings indicate that imidazole-conjugated 2-amino-4,6-diarylpyrimidines represent a potentially useful early-stage chemotype for antileishmanial optimization. Nevertheless, independent replicate experiments, complete activity profiling of the compound series, comparison with standard antileishmanial drugs, expanded cytotoxicity studies, and mechanistic validation are required before definitive lead selection can be established.

Keywords: *Leishmania*; 2-aminopyrimidine; imidazole; chalcone; guanidine hydrochloride; antileishmanial activity; intracellular amastigote; selectivity index.

INTRODUCTION

Leishmaniasis represents a therapeutically challenging parasitic disease because the clinically relevant parasite forms are distributed across distinct biological environments and because available drug classes are frequently constrained by toxicity, administration burden, cost, resistance or limited selectivity(1-5). The development of small molecules with improved parasite selectivity remains a rational strategy for early antileishmanial discovery. The present study was conceived around a medicinal-chemistry hypothesis rather than random screening: a pyrimidine core was selected as the central heteroaromatic scaffold, and imidazole substitution was introduced to generate a hybrid framework with potentially improved target interaction, lipophilicity and intracellular access. The resulting molecules were designed as 2-amino-4,6-diarylpyrimidines bearing an imidazole-containing aryl substituent at one side of the pyrimidine ring and a variable substituted phenyl group at the other side(5-10).

Relevant conflicts of interest/financial disclosures: The authors declare that the research was conducted in the absence of any commercial or financial relationships that could be construed as a potential conflict of interest.

The biological rationale for this scaffold class is linked to the importance of folate-associated pathways in Leishmania. Dihydrofolate reductase and pteridine reductase 1 are commonly considered parasite-relevant targets because they regulate reduced folate and pteridine pools required for nucleic-acid biosynthesis and other essential cellular functions. The design logic used in the supplied dataset assumes that targeting a single enzyme may be insufficient if a compensatory bypass mechanism remains active. In that context, compounds capable of interacting with pyrimidine-recognizing binding sites, or with related folate-pathway environments, are attractive starting points for lead exploration. The pyrimidine nucleus is structurally compatible with hydrogen-bonding interactions in nucleotide- and folate-associated protein pockets, while the 2-amino substituent can act as a donor element. The imidazole ring can contribute additional nitrogen atoms for polar recognition, modify the pKa profile of the molecule and influence binding geometry(10-15).

The substituted phenyl ring attached to the pyrimidine core was used as the main region for electronic and lipophilic variation. The compound series contains para-cyano, para-nitro, meta-chloro, ortho-chloro, 3,5-dichloro and 3,4-dimethoxy analogues. These substituents provide a small but useful chemical diversity set. Cyano and nitro groups introduce electron-withdrawing capacity and polarizability; chloro substituents increase hydrophobic character and may alter aryl ring orientation; dimethoxy substitution increases electron donation, hydrogen-bond acceptor capacity and steric bulk. The imidazole substituent at R1 was varied between methyl and ethyl, allowing a limited assessment of alkyl-chain size at the imidazole region. Although the original project rationale also mentions benzimidazole as a possible pharmacophore, the supplied experimental dataset for the present manuscript contains imidazole-conjugated compounds only. Accordingly, all conclusions in this manuscript are restricted to the imidazole-containing UG series(15-20).

The synthetic plan was constructed around a practical sequence that connects commercially accessible heterocycles and substituted acetophenones. The first transformation installs the imidazole unit onto 4-fluorobenzaldehyde through nucleophilic aromatic substitution under basic conditions. The resulting imidazole-substituted benzaldehyde intermediate is then converted to a chalcone through base-promoted condensation with a selected acetophenone. This step is valuable because chalcones are versatile alpha,beta-unsaturated ketone intermediates for subsequent heterocycle construction. The final cyclocondensation with guanidine hydrochloride forms the 2-aminopyrimidine nucleus. The route is operationally simple and gives direct access to a series of analogues because both the imidazole alkyl substituent and the acetophenone aryl substituent can be varied without changing the core synthetic logic.

For biological evaluation, the study prioritizes two levels of in vitro antileishmanial testing. A promastigote assay provides a first-pass viability screen against the extracellular parasite form. An intracellular amastigote assay is more biologically informative because amastigotes represent the mammalian intracellular stage of Leishmania and are located within host macrophages. A compound that appears active against promastigotes but loses potency in infected macrophages may lack cellular penetration, may be inactivated under intracellular conditions, or may act through a stage-specific mechanism that does not translate to the clinically relevant form. Therefore, the identification of UG-9 as active in the intracellular amastigote assay is a relevant observation. Cytotoxicity against RAW 264.7 macrophages was included to distinguish selective antileishmanial activity from nonspecific mammalian-cell toxicity.

2. MATERIALS AND METHODS

All chemical and biological methods below are written from the author-supplied experimental dataset. The chemical study used 4-fluorobenzaldehyde, 2-substituted imidazoles, anhydrous potassium carbonate, hexadecyltrimethylammonium bromide, N,N-dimethylformamide, methanol, sodium hydroxide, substituted acetophenones, guanidine hydrochloride and ethanol. Biological evaluation used Leishmania promastigote cultures, RAW 264.7 macrophages, suitable culture medium such as RPMI-1640 or DMEM according to cell and parasite requirements, fetal bovine serum, antibiotic solution, MTT or resazurin/Alamar Blue reagent, dimethyl sulfoxide as vehicle, phosphate-buffered saline, fixative and

Giemsa stain for intracellular parasite counting. Amphotericin B or miltefosine was identified as a positive control option in the supplied protocol framework, although comparative numerical control values were not supplied.

2.1 Compound design and nomenclature

The target compounds were designated UG-1 to UG-10. The general structure may be described as a 2-amino-4-aryl-6-[4-(2-R1-imidazol-1-yl)phenyl]pyrimidine derivative. R1 represents the alkyl substituent on the imidazole ring and was either methyl or ethyl. R2 represents the substituent on the phenyl ring derived from the corresponding substituted acetophenone. UG-1 to UG-6 contain the methyl-imidazole fragment, whereas UG-7 to UG-10 contain the ethyl-imidazole fragment. This design allows two structural comparisons: first, the influence of aryl substitution at the phenyl ring attached to the pyrimidine nucleus; second, the influence of methyl versus ethyl substitution at the imidazole region. The series is not large enough for a quantitative structure-activity relationship model, but it is adequate for initial qualitative structure-activity considerations.

2.2 General synthetic strategy

The synthesis was performed through three steps. Step 1 generated 4-(2-R1-imidazol-1-yl)benzaldehyde intermediates by reacting the selected 2-R1-substituted imidazole with 4-fluorobenzaldehyde in dry DMF. Anhydrous potassium carbonate was used to generate the nucleophilic imidazole species, and hexadecyltrimethylammonium bromide was used as a catalytic additive. The reaction mixture was heated at 100 °C for 28 h and monitored by thin-layer chromatography. After completion, the mixture was cooled and poured onto crushed ice. The separated solid was filtered, washed with cold water, dried and recrystallized from methanol. This step installed the imidazole pharmacophore on the para-formyl phenyl ring while preserving the aldehyde functionality needed for chalcone formation.

2.3 Synthesis of chalcone intermediates

Step 2 involved Claisen-Schmidt condensation. The imidazole-substituted benzaldehyde intermediate was dissolved in methanol, and an equimolar amount of the selected substituted acetophenone was added. A 10% methanolic sodium hydroxide solution was added dropwise with continuous stirring at room temperature. The reaction mixture was stirred for approximately 1 h and monitored by TLC. After completion, the mixture was poured into cold water or ice-water. The precipitated chalcone intermediate was filtered, washed with a cold methanol-water mixture, dried and recrystallized from methanol. The formation of chalcone intermediates is mechanistically important because it introduces the alpha,beta-unsaturated carbonyl system that subsequently participates in pyrimidine ring formation.

2.4 Synthesis of 2-aminopyrimidine derivatives

Step 3 converted the chalcone intermediates into the final 2-aminopyrimidine derivatives. Each chalcone was added to a solution of guanidine hydrochloride in 5% ethanolic sodium hydroxide. The reaction mixture was heated under reflux at 75 °C for approximately 6 h and monitored by TLC. After completion, the reaction mixture was cooled to room temperature and poured onto crushed ice. The solid product was collected by filtration, washed with cold water, dried and recrystallized from ethanol followed by methanol where required. The transformation likely proceeds through nucleophilic addition of guanidine to the activated enone system, followed by cyclization, dehydration and aromatization to generate the 2-aminopyrimidine core.

2.5 Purification and physicochemical assessment

The crude UG derivatives were purified by recrystallization using methanol, ethanol or sequential ethanol-methanol systems depending on compound solubility. Recrystallization was used to remove unreacted starting materials, inorganic salts and minor by-products. Melting points were determined by the open capillary method.

2.6 Thin-layer chromatography

Thin-layer chromatography was used for reaction monitoring and preliminary purity assessment. TLC allowed visualization of the disappearance of starting materials and the appearance of products during aldehyde formation, chalcone synthesis, and pyrimidine cyclization. The chromatographic plates

were developed using a chloroform–methanol mobile phase and visualized under ultraviolet light. Product formation was inferred from the appearance of a new spot with an Rf value different from that of the corresponding starting material. After purification, the presence of a single major spot was considered preliminary evidence of acceptable purity. Because Rf values are influenced by the stationary phase, mobile-phase composition, chamber saturation, plate activation, and detection method, the exact chloroform-to-methanol ratio should be reported for reproducibility.

2.7 FT-IR Characterization of Synthesized Compounds

The synthesized compounds were characterized using FT-IR spectroscopy. The FT-IR spectra were recorded using the KBr pellet method and interpreted based on major diagnostic functional groups. Bands assigned to NH_2 stretching were observed in the region of 3440–3320 cm^{-1}. Aromatic C–H stretching appeared near 3035–3038 cm^{-1}. Aliphatic C–H stretching bands were observed around 2920 cm^{-1} for methyl-substituted analogues and within 2960–2870 cm^{-1} for ethyl-substituted analogues. Cyano-containing derivatives showed characteristic C≡N stretching bands in the 2220–2240 cm^{-1} region. Pyrimidine-associated C=N stretching appeared around 1640–1600 cm^{-1}, while aromatic C=C stretching vibrations were assigned to the 1585–1510 cm^{-1} region. Chloro-substituted analogues exhibited C–Cl stretching bands between 780 and 700 cm^{-1}. Methoxy-substituted derivatives displayed characteristic bands attributable to Ar–OCH_3 and C–O–C stretching vibrations.

2.8 Promastigote viability assay

The initial in vitro antileishmanial screen was performed using Leishmania promastigotes. Log-phase promastigotes were distributed into sterile microtitre plates and exposed to graded concentrations of test compounds. Untreated parasite control, vehicle control, media blank, compound blank and a positive control drug were included as assay controls. In the MTT format, viable promastigotes reduce yellow MTT to purple formazan, which is solubilized before absorbance measurement using a microplate reader. In the resazurin/Alamar Blue format, metabolically active parasites reduce blue resazurin to fluorescent or pink resorufin. A lower absorbance or fluorescence signal relative to the vehicle control indicates reduced parasite viability. Percentage inhibition is calculated relative to the vehicle control, and IC50 values are derived from concentration-response curves. Exact parasite density, concentration range, incubation time, plate format, wavelength or fluorescence settings and regression model were not supplied.

2.9 Intracellular amastigote assay

The intracellular amastigote assay was used to confirm activity under a biologically more relevant condition. RAW 264.7 macrophages were infected with promastigote forms of Leishmania donovani. After parasite internalization and establishment of intracellular infection, extracellular parasites were removed and infected macrophages were treated with graded concentrations of the test compounds. Following treatment, cells were fixed, stained and examined microscopically. The percentage of infected macrophages, number of intracellular amastigotes per infected macrophage, infection index, percentage inhibition and IC50 values can be calculated from microscopic counts. The supplied dataset identifies the intracellular amastigote IC50 of UG-9 but does not provide the multiplicity of infection, infection duration, treatment duration, number of macrophages counted per replicate, blinding procedure or replicate number. These details are essential for reproducibility and should be added before submission.

2.10 Cytotoxicity and selectivity index

Cytotoxicity was evaluated against RAW 264.7 macrophages to assess whether the observed antileishmanial activity was selective for the parasite or attributable to nonspecific mammalian-cell toxicity. Macrophages were exposed to graded concentrations of test compound, and viability was assessed using a metabolic assay. The CC50 value represents the concentration that reduces mammalian-cell viability by 50%. Selectivity index was calculated as CC50 divided by parasite IC50. Two selectivity indices can be calculated for UG-9: one using the promastigote IC50 and one using the intracellular amastigote IC50. The intracellular amastigote-based selectivity index is the more relevant metric for lead

prioritization because it uses the mammalian-stage parasite form.

2.11 Data treatment and reporting

The supplied numerical biological dataset contains IC50 values for UG-9 against promastigotes and intracellular amastigotes and a CC50 value against RAW 264.7 macrophages. Full dose-response curves, replicate-level values, measures of variability and positive-control values were not supplied. Therefore, the results are reported as preliminary point estimates. In a final manuscript, IC50 and CC50 values should be calculated by nonlinear regression from at least three independent experiments, expressed with standard deviation, standard error or 95% confidence intervals, and compared with a reference drug measured under the same assay conditions. Compound-only controls are also necessary because colored or redox-active molecules can interfere with MTT and resazurin readouts.

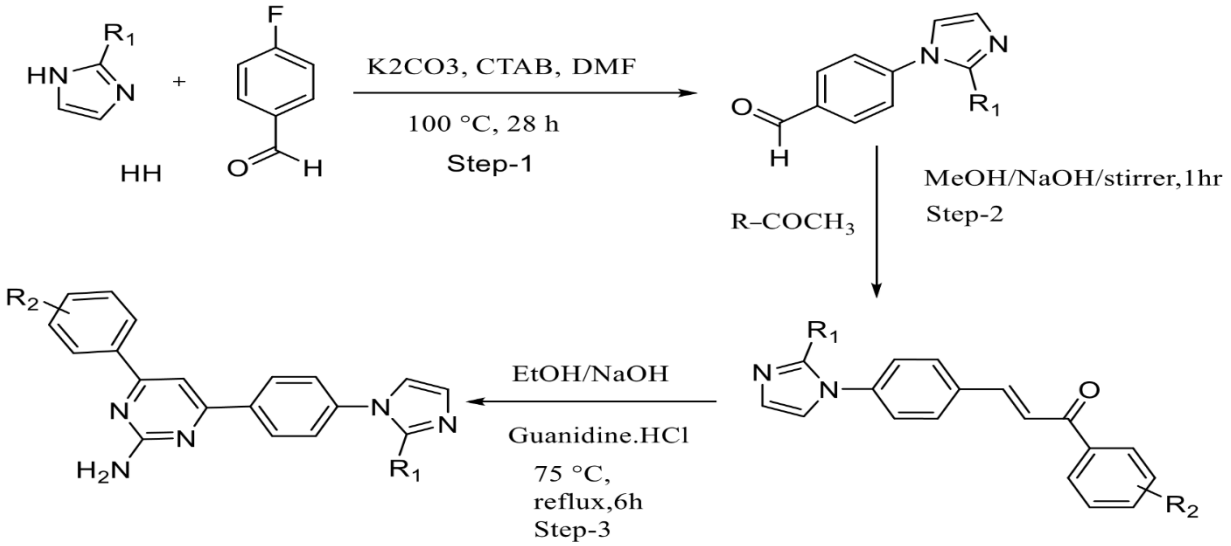

Scheme 1. Synthetic route for imidazole-conjugated 2-amino-4,6-diarylpyrimidine derivatives UG-1 to UG-10. R1 = CH3 or C2H5; R2 = substituted phenyl group.

3. RESULTS

The synthetic series comprised ten UG derivatives with systematic variation at R1 and R2. Isolated yields ranged from 55% to 85%, indicating that the synthetic sequence was generally productive across both methyl- and ethyl-imidazole analogues. The highest yields were observed for UG-4 and UG-10, both bearing an ortho-chloro substituent on the aryl ring, with yields of 85%. UG-7, the ethyl-imidazole analogue bearing a para-cyano group, gave the lowest reported yield at 55%. The remaining compounds were obtained in moderate to good yields. The reaction sequence tolerated electron-withdrawing cyano and nitro substituents, chloro substitution and electron-rich dimethoxy substitution.

Compound	R1	R2	Yield (%)	Rf
UG-1	CH_3	4-CN	78	0.80
UG-2	CH_3	4-NO_2	67	0.70
UG-3	CH_3	3-Cl	80	0.55
UG-4	CH_3	2-Cl	85	0.50

UG-5	CH_3	3,5-Cl_2	66	0.130
UG-6	CH_3	3,4-$(OCH_3)_2$	75	0.70
UG-7	C_2H_5	4-CN	55	0.80
UG-8	C_2H_5	4-NO_2	67	0.78
UG-9	C_2H_5	3-Cl	80	0.32
UG-10	C_2H_5	2-Cl	85	0.186

Table 1. Substitution pattern, isolated yield and TLC Rf values of synthesized UG derivatives.

3.1 Synthetic route and reaction outcome

The overall synthetic scheme is shown in Scheme 1. The route begins with formation of imidazole-containing aldehyde intermediates, proceeds through chalcone formation and terminates in guanidine-mediated cyclization to 2-aminopyrimidines. The sequence is attractive for analogue generation because the two diversity points are introduced through readily varied imidazole and acetophenone components. The first step is expected to be sensitive to the nucleophilicity and steric demand of the imidazole substrate. The second step is influenced by the reactivity of the aldehyde and acetophenone, while the third step depends on the electrophilic character and conformational accessibility of the chalcone intermediate. The successful preparation of all ten final compounds indicates that no substituent in this small set prevented formation of the target pyrimidine framework.

3.2 TLC profile

The Rf values of the synthesized compounds ranged from 0.130 to 0.80 using **chloroform–methanol** as the mobile phase. The highest Rf values were observed for UG-1 and UG-7, both *para*-cyano analogues, with an Rf value of 0.80. The nitro-substituted derivatives UG-2 and UG-8 showed Rf values of 0.70 and 0.78, respectively. Among the chloro-substituted analogues, UG-3, UG-4, UG-9, and UG-10 exhibited Rf values of 0.55, 0.50, 0.32, and 0.186, respectively. UG-5, containing a 3,5-dichloro substituent, showed the lowest Rf value of 0.130, whereas the 3,4-dimethoxy-substituted derivative UG-6 showed an Rf value of 0.70. These differences indicate that chromatographic mobility was influenced by both aryl substitution and the alkyl substituent attached to the imidazole moiety. The observed Rf variation was useful for monitoring reaction completion, distinguishing the synthesized derivatives, and supporting preliminary purity assessment.

3.3 FT-IR characterization

FT-IR spectra provided functional-group-level evidence supporting the proposed structures. All compounds showed broad bands in the 3440-3320 cm-1 region assigned to the 2-amino group. Aromatic C-H bands around 3035 cm-1 and aromatic C=C bands around 1585-1510 cm-1 were consistent with the presence of multiple aryl and heteroaryl rings. C=N stretching near 1640-1600 cm-1 supported the presence of imine-like heteroaromatic linkages in the pyrimidine and imidazole framework. Cyano-substituted compounds UG-1 and UG-7 showed characteristic C≡N absorption near 2225 cm-1 or 2220-2240 cm-1. Nitro-substituted UG-2 showed asymmetric and symmetric nitro bands in the 1520-1550 and 1340-1370 cm-1 regions. Chloro-substituted analogues showed C-Cl bands between 780 and 700 cm-1. UG-6, the dimethoxy analogue, exhibited Ar-OCH3 and C-O-C bands. FT-IR alone cannot confirm regioisomeric identity, but the spectral pattern is consistent with the proposed substitution classes.

Compound	Key FT-IR bands reported (KBr, cm-1)
UG-1	3440-3320 (NH2), 3038 (Ar-C-H), 2920 (CH3 C-H), 2225 (C≡N), 1640 (C=N), 1585-1510 (Ar C=C), 1240-1120 (C-N), 830 (p-disubstituted Ar C-H bend)
UG-2	3440-3320 (NH2), 3035 (Ar-C-H), 2920 (CH3 C-H), 1640-1600 (C=N), 1585-1510 (Ar C=C), 1520-1550 and 1340-1370 (NO2), 1240-1120 (C-N)
UG-3	3440-3320 (NH2), 3035 (Ar-C-H), 2920 (CH3 C-H), 1640-1600 (C=N), 1585-1510 (Ar C=C), 1240-1120 (C-N), 760-700 (C-Cl)
UG-4	3440-3320 (NH2), 3035 (Ar-C-H), 2920 (CH3 C-H), 1640-1600 (C=N), 1585-1510 (Ar C=C), 1240-1120 (C-N), 760-700 (C-Cl)
UG-5	3440-3320 (NH2), 3035 (Ar-C-H), 2920 (CH3 C-H), 1640-1600 (C=N), 1585-1510 (Ar C=C), 1240-1120 (C-N), 780-700 (C-Cl)
UG-6	3440-3320 (NH2), 3035 (Ar-C-H), 1640-1600 (C=N), 1585-1510 (Ar C=C), 1260-1240 (Ar-OCH3 C-O), 1160-1020 (C-O-C), 1240-1120 (C-N)
UG-7	3440-3320 (NH2), 3035 (Ar-C-H), 2960-2870 (C2H5 C-H), 2220-2240 (C≡N), 1640-1600 (C=N), 1585-1510 (Ar C=C), 1240-1120 (C-N)
UG-8	3440-3320 (NH2), 3035 (Ar-C-H), 2960-2870 (C2H5 C-H), 1640-1600 (C=N), 1585-1510 (Ar C=C); NO2 bands not explicitly reported in the supplied data
UG-9	3440-3320 (NH2), 3035 (Ar-C-H), 2960-2870 (C2H5 C-H), 1640-1600 (C=N), 1585-1510 (Ar C=C), 1240-1120 (C-N), 760-700 (C-Cl)
UG-10	3440-3320 (NH2), 3035 (Ar-C-H), 2960-2870 (C2H5 C-H), 1640-1600 (C=N), 1585-1510 (Ar C=C), 1240-1120 (C-N), 760-700 (C-Cl)

Table 2. Diagnostic FT-IR assignments for UG-1 to UG-10.

3.4 Biological evaluation of UG-9

The supplied biological data identify UG-9 as the most promising compound in the UG series. UG-9 contains an ethyl substituent at the imidazole region and a 3-chlorophenyl substituent on the aryl ring attached to the pyrimidine nucleus. In the promastigote viability assay, UG-9 produced an IC50 value of 11.2 micromolar. In the intracellular amastigote assay, UG-9 produced an IC50 value of 8.6 micromolar. The lower intracellular amastigote IC50 indicates that the compound retained activity against the parasite stage located within macrophages and may be more potent under the intracellular assay conditions than against promastigotes. Cytotoxicity testing against RAW 264.7 macrophages gave a CC50 value of 126.4 micromolar. This value is substantially higher than the antileishmanial IC50 values, supporting a preliminary selectivity signal. The selectivity index calculated using the intracellular amastigote IC50 was 14.7. Using the promastigote IC50, the selectivity index was approximately 11.3. These values justify further study of UG-9 as an early-stage lead candidate.

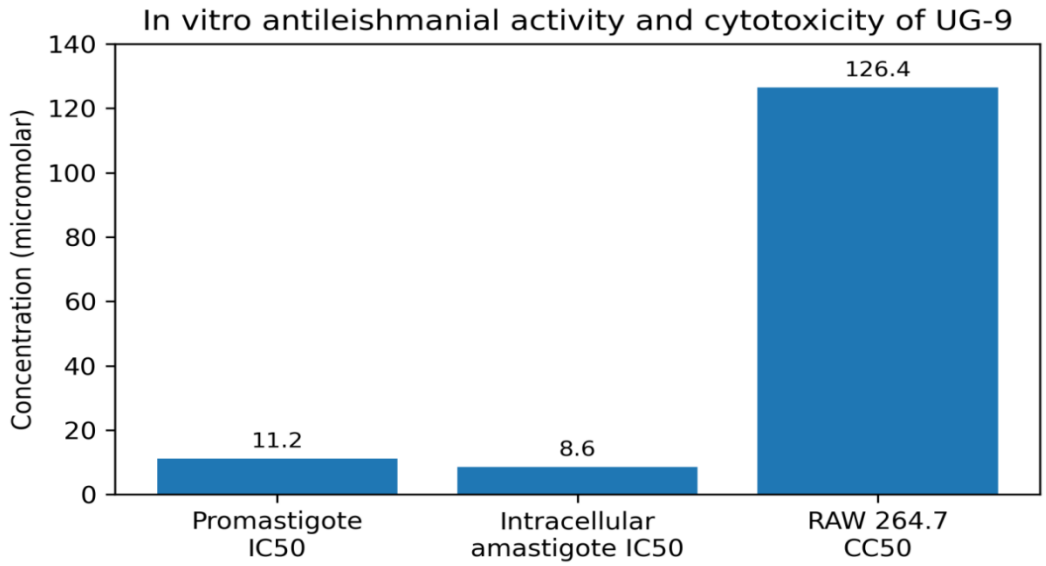

Figure 2. In vitro antileishmanial activity and RAW 264.7 cytotoxicity profile of UG-9 based on supplied IC50 and CC50 values.

Parameter	UG-9 value	Interpretation
Leishmania promastigote IC50	11.2 micromolar	Primary extracellular-stage inhibition
Intracellular amastigote IC50	8.6 micromolar	Activity retained in the macrophage infection model
RAW 264.7 macrophage CC50	126.4 micromolar	Lower mammalian-cell cytotoxicity than parasite inhibition values
Selectivity index using promastigote IC50	11.3	CC50/promastigote IC50
Selectivity index using amastigote IC50	14.7	CC50/intracellular amastigote IC50

Table 3. Reported antileishmanial and cytotoxicity profile of UG-9.

3.6 Structure-activity considerations

A rigorous structure-activity relationship cannot be established from the available dataset because full IC50 values for UG-1 to UG-8 and UG-10 were not supplied. Nonetheless, the identification of UG-9 as the leading compound supports several hypotheses. First, the ethyl substituent on the imidazole ring may provide a favorable balance between hydrophobicity and steric demand compared with methyl analogues. Second, the 3-chloro substituent may position the phenyl ring in a favorable orientation or increase lipophilic interactions with parasite-associated molecular environments. Third, the 2-amino pyrimidine core may provide a hydrogen-bonding pattern compatible with parasite enzyme pockets or other intracellular targets. These hypotheses require confirmation through complete activity profiling of all analogues, enzyme inhibition assays, computational docking supported by experimental validation and expanded cytotoxicity testing.

3.7 Comparison of promastigote and intracellular activity

The observation that UG-9 exhibited a lower IC50 against intracellular amastigotes than against promastigotes is important but must be interpreted carefully. A lower amastigote IC50 can indicate genuine stage-specific sensitivity, improved compound accumulation in macrophages, intracellular activation, or methodological differences between the two assays. It can also arise from assay endpoint differences, host-cell effects on parasite metabolism or variability in concentration-response fitting. Therefore, the finding should be treated as encouraging rather than conclusive. Confirmation requires repeat testing with matched concentration ranges, identical exposure durations where feasible, appropriate vehicle controls, microscopic validation and comparison with a reference drug in the same assay run. If reproducible, this intracellular activity profile would be advantageous because amastigotes represent the clinically relevant form of the parasite in mammalian hosts.

3.8 Selectivity interpretation

The intracellular amastigote-based selectivity index of 14.7 indicates that UG-9 was approximately 14.7-fold more inhibitory to intracellular Leishmania amastigotes than toxic to RAW 264.7 macrophages under the reported conditions. This supports a preliminary therapeutic window but does not establish safety. RAW 264.7 cells are an immortalized macrophage line and may not represent the sensitivity of primary macrophages, hepatocytes, cardiomyocytes or renal epithelial cells. In addition, CC50 values based on metabolic readouts may overestimate or underestimate true cytotoxicity depending on compound interference and mitochondrial effects. A credible preclinical safety assessment would require additional mammalian cell types, hemolysis screening where relevant, mitochondrial toxicity testing and early in vitro ADME profiling. Nevertheless, the supplied CC50 and IC50 values support continued investigation of UG-9 rather than immediate rejection for nonspecific toxicity.

4. DISCUSSION

The current dataset supports the feasibility of synthesizing imidazole-conjugated 2-aminopyrimidine derivatives through a concise and adaptable route. From a medicinal chemistry perspective, the route is useful because it separates the molecule into three tunable regions: the imidazole alkyl substituent, the central pyrimidine pharmacophore and the substituted aryl ring. Such modularity is valuable in lead optimization because substituent changes can be introduced without redesigning the entire synthetic sequence. The reported yields indicate that the route tolerates a range of electron-withdrawing and electron-donating substituents. The practical use of recrystallization rather than chromatographic purification is also advantageous for gram-scale exploratory synthesis, provided that final purity can later be confirmed by validated analytical methods.

4.1 Chemical significance of the synthetic design

The use of chalcone intermediates is a strategic feature of the synthetic design. Chalcones provide a conjugated enone system that can react with guanidine to form aminopyrimidines. This enables construction of a pyrimidine core while simultaneously preserving aryl substituent diversity. The first step, nucleophilic displacement on 4-fluorobenzaldehyde, creates a para-substituted aldehyde intermediate that acts as a common precursor. The para-phenylene linker introduces spatial separation between the imidazole ring and pyrimidine nucleus, potentially allowing both regions to participate in binding or physicochemical modulation. The final 2-aminopyrimidine product contains multiple nitrogen atoms, aromatic surfaces and substituent-dependent hydrophobic regions, all of which may influence parasite uptake, target engagement and selectivity.

4.2 Biological relevance of the intracellular amastigote assay

The intracellular amastigote result is the most biologically relevant component of the dataset. Promastigote assays are useful for screening because they are technically simpler and allow rapid detection of antiparasitic activity. However, the promastigote form does not fully reproduce the intracellular

conditions encountered by Leishmania in mammalian macrophages. A compound must reach intracellular parasites without excessive host-cell toxicity to be considered a serious lead. UG-9 showed an intracellular amastigote IC50 of 8.6 micromolar and a macrophage CC50 of 126.4 micromolar, giving a selectivity index of 14.7. This is a meaningful preliminary signal, especially because selectivity is often a limiting factor in antileishmanial drug discovery. Still, the absence of positive-control values prevents direct potency benchmarking against amphotericin B, miltefosine or other standard drugs.

4.3 Potential mechanisms and target hypotheses

The project hypothesis proposes that the imidazole-pyrimidine hybrids may interfere with parasite folate metabolism, particularly through DHFR/PTR1-related pathways. This is a plausible medicinal-chemistry hypothesis because the pyrimidine core resembles heteroaromatic motifs found in compounds interacting with nucleotide or folate-associated binding environments. However, the current dataset does not include enzyme inhibition assays, binding studies, docking validation, rescue experiments or metabolomic evidence. Therefore, DHFR/PTR1 involvement should be considered a hypothesis rather than a demonstrated mechanism. Alternative mechanisms are possible, including disruption of mitochondrial function, redox imbalance, membrane perturbation, interference with other nucleic-acid-associated enzymes, or compound-induced stress pathways. Mechanistic clarification would require target-based biochemical assays, resistant-line profiling, cellular thermal shift assays, metabolite rescue studies and orthogonal phenotypic readouts.

4.4 Preliminary SAR hypotheses

The most active supplied compound, UG-9, combines an ethyl-imidazole fragment with a meta-chloro aryl substituent. This combination may improve the balance between hydrophobicity and polar heteroatom density. The ethyl group may enhance membrane permeability or fit a hydrophobic region adjacent to the imidazole binding area. The meta-chloro substituent may contribute to lipophilic contacts, modify aryl electronics or influence the preferred conformation of the diarylpyrimidine system. The lower activity of other analogues cannot be evaluated quantitatively because their full IC50 values were not supplied. Nevertheless, a logical next analogue set would include fluoro, bromo, trifluoromethyl, methyl, methoxy and pyridyl variants at the R2 aryl position, as well as additional small alkyl substituents at the imidazole region. Such analogues would help determine whether UG-9 activity depends on hydrophobicity, electronic withdrawal, steric position, or a specific halogen effect.

4.5 Future optimization strategy

UG-9 should be treated as an early-stage lead rather than a final candidate. The compound should then be retested in promastigote and intracellular amastigote assays with full concentration-response curves. Parallel cytotoxicity should be performed in RAW 264.7 cells and at least one additional mammalian cell model. If the activity is confirmed, enzyme assays against Leishmania DHFR and PTR1 should be used to test the folate pathway hypothesis. Mechanistic phenotypic assays should evaluate mitochondrial membrane potential, reactive oxygen species, cell-cycle disturbance, membrane integrity and apoptosis-like features. Chemical optimization should focus on modifying the R2 aryl substituent, the imidazole alkyl group and the para-phenylene linker while monitoring solubility, metabolic stability and selectivity.

CONCLUSION

A focused series of ten imidazole-conjugated 2-amino-4,6-diarylpyrimidine derivatives, designated UG-1 to UG-10, was designed and synthesized through a three-step sequence involving imidazole substitution of 4-fluorobenzaldehyde, Claisen–Schmidt condensation to form chalcone intermediates, and guanidine-mediated pyrimidine cyclization. The synthetic procedure successfully accommodated methyl- and ethyl-substituted imidazole fragments together with cyano, nitro, chloro, dichloro, and dimethoxy aryl substituents. The derivatives were obtained in yields ranging from 55% to 85%, while their TLC Rf values ranged from 0.130 to 0.80. FT-IR analysis provided preliminary functional-group-level support for the formation of the proposed substitution classes.

Among the available biological results, UG-9 emerged as the most promising derivative. The compound exhibited IC_{50} values of 11.2 µM against

Leishmania promastigotes and 8.6 µM against intracellular amastigotes, together with a CC_{50} value of 126.4 µM against RAW 264.7 macrophages. The corresponding intracellular amastigote-based selectivity index of 14.7 indicates a preliminary degree of parasite selectivity under the reported experimental conditions. However, these results represent early-stage evidence and do not establish UG-9 as a validated therapeutic candidate.

Further investigation should include independent synthesis and biological replication, complete concentration–response evaluation of all UG derivatives, statistical analysis of IC_{50} and CC_{50} values, direct comparison with standard antileishmanial drugs, evaluation in additional mammalian cell models, and experimental assessment of the proposed DHFR/PTR1-related mechanism. Subject to such validation, UG-9 may serve as a rational starting point for the continued optimization of imidazole-conjugated pyrimidine derivatives as antileishmanial agents.

REFERENCES

1. Burza S, Croft SL, Boelaert M. Leishmaniasis. Lancet. 2018;392(10151):951–970. doi:10.1016/S0140-6736(18)31204-2.
2. Croft SL, Coombs GH. Leishmaniasis current chemotherapy and recent advances in the search for novel drugs. Trends Parasitol. 2003;19(11):502–508. doi:10.1016/j.pt.2003.09.008.
3. Croft SL, Sundar S, Fairlamb AH. Drug resistance in leishmaniasis. Clin Microbiol Rev. 2006;19(1):111–126. doi:10.1128/CMR.19.1.111-126.2006.
4. Uliana SRB, Trinconi CT, Coelho AC. Chemotherapy of leishmaniasis: present challenges. Parasitology. 2018;145(4):464–480. doi:10.1017/S0031182016002523.
5. Nagle AS, Khare S, Kumar AB, Supek F, Buchynskyy A, Mathison CJN, et al. Recent developments in drug discovery for leishmaniasis and human African trypanosomiasis. Chem Rev. 2014;114(22):11305–11347. doi:10.1021/cr500365f.
6. Nare B, Luba J, Hardy LW, Beverley S. New approaches to Leishmania chemotherapy: pteridine reductase 1 as a target and modulator of antifolate sensitivity. Parasitology. 1997;114 Suppl:S101–S110. doi:10.1017/S0031182097001133.
7. Tulloch LB, Martini VP, Iulek J, Huggan JK, Lee JH, Gibson CL, et al. Structure-based design of pteridine reductase inhibitors targeting African sleeping sickness and the leishmaniases. J Med Chem. 2010;53(1):221–229. doi:10.1021/jm901059x.
8. Mpamhanga CP, Spinks D, Tulloch LB, Shanks EJ, Robinson DA, Collie IT, et al. One scaffold, three binding modes: novel and selective pteridine reductase 1 inhibitors derived from fragment hits discovered by virtual screening. J Med Chem. 2009;52(14):4454–4465. doi:10.1021/jm900414x.
9. Khalaf AI, Huggan JK, Suckling CJ, Gibson CL, Stewart K, Giordani F, et al. Structure-based design and synthesis of antiparasitic pyrrolopyrimidines targeting pteridine reductase 1. J Med Chem. 2014;57(15):6479–6494. doi:10.1021/jm500483b.
10. Teixeira BVF, Teles ALB, da Silva SG, Brito CCB, de Freitas HF, Pires ABL, et al. Dual and selective inhibitors of pteridine reductase 1 and dihydrofolate reductase-thymidylate synthase from Leishmania chagasi. J Enzyme Inhib Med Chem. 2019;34(1):1439–1450. doi:10.1080/14756366.2019.1651311.
11. Patle SK, Kawathekar N, Zaveri M, Kamaria P. Synthesis and evaluation of 2,4,6-trisubstituted pyrimidine derivatives as novel antileishmanial agents. Med Chem Res. 2013;22(4):1756–1761. doi:10.1007/s00044-012-0167-y.
12. Kumar R, Singh R, et al. Imidazo[1,2-a]pyrimidine as a new antileishmanial pharmacophore against Leishmania amazonensis promastigotes and amastigotes. ACS Omega. 2023;8(43):40613–40621. doi:10.1021/acsomega.3c05441.
13. Tonelli M, Gabriele E, Piazza F, Basilico N, Parapini S, Tasso B, et al. Benzimidazole derivatives endowed with potent antileishmanial activity. J Enzyme Inhib Med Chem. 2018;33(1):210–226. doi:10.1080/14756366.2017.1410480.
14. Sánchez-Salgado JC, Bilbao-Ramos P, Dea-Ayuela MA, Hernández-Luis F, Bolás-Fernández F, Medina-Franco JL, et al. Systematic search for

benzimidazole compounds and derivatives with antileishmanial effects. Mol Divers. 2018;22(4):779–790. doi:10.1007/s11030-018-9830-7.

15. de Mello MVP, Abrahim-Vieira BA, Domingos TFS, de Jesus JB, de Sousa ACC, Rodrigues CR, et al. A comprehensive review of chalcone derivatives as antileishmanial agents. Eur J Med Chem. 2018;150:920–929. doi:10.1016/j.ejmech.2018.03.047.
16. Boeck P, Falcão CAB, Leal PC, Yunes RA, Cechinel Filho V, Torres-Santos EC, et al. Synthesis of chalcone analogues with increased antileishmanial activity. Bioorg Med Chem. 2006;14(5):1538–1545. doi:10.1016/j.bmc.2005.10.005.
17. Vermeersch M, da Luz RI, Toté K, Timmermans JP, Cos P, Maes L. In vitro susceptibilities of Leishmania donovani promastigote and amastigote stages to antileishmanial reference drugs: practical relevance of stage-specific differences. Antimicrob Agents Chemother. 2009;53(9):3855–3859. doi:10.1128/AAC.00548-09.
18. De Muylder G, Ang KKH, Chen S, Arkin MR, Engel JC, McKerrow JH. A screen against Leishmania intracellular amastigotes: comparison to a promastigote screen and identification of a host cell-specific hit. PLoSNegl Trop Dis. 2011;5(7):e1253. doi:10.1371/journal.pntd.0001253.
19. Mosmann T. Rapid colorimetric assay for cellular growth and survival: application to proliferation and cytotoxicity assays. J Immunol Methods. 1983;65(1–2):55–63. doi:10.1016/0022-1759(83)90303-4.
20. Corral MJ, González E, Cuquerella M, Alunda JM. Improvement of 96-well microplate assay for estimation of cell growth and inhibition of Leishmania with Alamar Blue. J Microbiol Methods. 2013;94(2):111–116. doi:10.1016/j.mimet.2013.05.012.

HOW TO CITE: Dipraj Kochak*, Archana Tiwari, Shikha Nagle, Dishant Gupta, Design, Synthesis, Characterization And In Vitro Antileishmanial Evaluation Of 2,4,6-Substituted Pyrimidine Derivatives Conjugated With Imidazole Moieties, Int. J. Sci. R. Tech., 2026, 3 (8), 1-12. https://doi.org/10.5281/zenodo.21739137